Supporting information for

Low-velocity-favored transition radiation

Jialin Chen, Ruoxi Chen, Fuyang Tay, Zheng Gong, Hao Hu, Yi Yang, Xinyan Zhang, Chan Wang, Ido Kaminer, Hongsheng Chen, Baile Zhang, and Xiao Lin

Supplementary Information Guide:

Section S1. Derivation of transition radiation from a uniaxial slab

Below we show the detailed derivation of transition radiation [1-5]. As shown in Fig. 1, a swift electron with a charge of q moves along the $+\hat{z}$ direction and perpendicularly penetrates through an epsilon-near-

zero uniaxial slab with a thickness d. The uniaxial slab (denoted as region 2), for example, can be constructed by the hexagonal BN with a relative permittivity of $[\varepsilon_\perp, \varepsilon_\perp, \varepsilon_\mathrm{z}]$, which has $\varepsilon_\mathrm{z} \to 0$ around the frequency of 24.5 THz. For illustration, both the superstrate (region 1) and the substrate (region 3) are free space with a relative permittivity of $\varepsilon_1 = \varepsilon_3 = 1$.

Within the framework of macroscopic Maxwell equations, the induced current by a moving electron with a velocity v can be expressed as

$$\bar{J}^q(\bar{r}, t) = \hat{z} q v \delta(x)\delta(y)\delta(z - vt) \tag{S1}$$

Using the Fourier transformation (or the plane wave expansion), the expressions for the current, the electric field, and the magnetic field are obtained as follows [1-5]:

$$\bar{J}^\mathrm{q}(\bar{r}, t) = \int \hat{z} j^\mathrm{q}_{\omega,\bar{\kappa}_\perp}(z) e^{i(\bar{\kappa}_\perp \cdot \bar{r}_\perp - \omega t)} d\bar{\kappa}_\perp d\omega \tag{S2}$$

$$\bar{E}(\bar{r}, t) = \int \bar{E}_{\omega,\bar{\kappa}_\perp}(z)\, e^{i(\bar{\kappa}_\perp \cdot \bar{r}_\perp - \omega t)} d\bar{\kappa}_\perp d\omega \tag{S3}$$

$$\bar{H}(\bar{r}, t) = \int \bar{H}_{\omega,\bar{\kappa}_\perp}(z)\, e^{i(\bar{\kappa}_\perp \cdot \bar{r}_\perp - \omega t)} d\bar{\kappa}_\perp d\omega \tag{S4}$$

where $\bar{\kappa}_\perp = \hat{x}\kappa_\mathrm{x} + \hat{y}\kappa_\mathrm{y}$ is the wavevector component perpendicular to the electron velocity. From equations (S1-S2), we further have

$$j^q_{\omega,\bar{\kappa}_\perp}(z) = \frac{q}{(2\pi)^3} e^{i\frac{\omega}{v}z} \tag{S5}$$

Furthermore, the boundary conditions require

$$\hat{n} \times (\bar{E}_{1\perp} - \bar{E}_{2\perp})|_{\mathrm{z}=0} = 0 \tag{S6}$$

$$\hat{n} \times (\bar{H}_{1\perp} - \bar{H}_{2\perp})|_{\mathrm{z}=0} = 0 \tag{S7}$$

$$\hat{n} \times (\bar{E}_{2\perp} - \bar{E}_{3\perp})|_{\mathrm{z}=\mathrm{d}} = 0 \tag{S8}$$

$$\hat{n} \times (\bar{H}_{2\perp} - \bar{H}_{3\perp})|_{\mathrm{z}=\mathrm{d}} = 0 \tag{S9}$$

By enforcing these boundary conditions in equations (S6-S9), the distribution of the excited magnetic fields in regions 1-3 can be calculated. After some derivations, we show these solutions in the cylindrical coordinate of $\rho\phi z$ [3, 5] as follows

$$\bar{H}_j(\bar{r}, t) = \bar{H}_j^\mathrm{q}(\bar{r}, t) + \bar{H}_j^\mathrm{r}(\bar{r}, t) \ (j = 1, 2 \text{ or } 3) \tag{S10}$$

$$\bar{H}_1^\mathrm{q}(\bar{r}, t) = \hat{\phi} \int_{-\infty}^{+\infty} d\omega \frac{iq}{8\pi} \sqrt{\frac{\omega^2}{c^2}\varepsilon_1 - \frac{\omega^2}{v^2}}\, H_1^{(1)}\Big(\sqrt{\frac{\omega^2}{c^2}\varepsilon_1 - \frac{\omega^2}{v^2}}\,\rho\Big) e^{i(\frac{\omega}{v}z - \omega t)} \tag{S11}$$

$$\bar{H}_2^{\mathrm{q}}(\bar{r},t)=\hat{\phi}\int_{-\infty}^{+\infty}d\omega\,\frac{iq}{8\pi}\sqrt{\frac{\omega^2}{c^2}\varepsilon_{\mathrm{z}}-\frac{\omega^2}{v^2}\frac{\varepsilon_{\mathrm{z}}}{\varepsilon_{\perp}}}\,H_1^{(1)}\!\left(\sqrt{\frac{\omega^2}{c^2}\varepsilon_{\mathrm{z}}-\frac{\omega^2}{v^2}\frac{\varepsilon_{\mathrm{z}}}{\varepsilon_{\perp}}}\,\rho\right)e^{i(\frac{\omega}{v}z-\omega t)} \tag{S12}$$

$$\bar{H}_3^{\mathrm{q}}(\bar{r},t)=\hat{\phi}\int_{-\infty}^{+\infty}d\omega\,\frac{iq}{8\pi}\sqrt{\frac{\omega^2}{c^2}\varepsilon_3-\frac{\omega^2}{v^2}}\,H_1^{(1)}\!\left(\sqrt{\frac{\omega^2}{c^2}\varepsilon_3-\frac{\omega^2}{v^2}}\,\rho\right)e^{i(\frac{\omega}{v}z-\omega t)} \tag{S13}$$

$$\bar{H}_1^{\mathrm{r}}(\bar{r},t)=\hat{\phi}\int_{-\infty}^{+\infty}d\omega\int_0^{+\infty}d\kappa_{\perp}\,\frac{iq}{\omega\varepsilon_0(2\pi)^3}\,a_1(-\omega\varepsilon_0\varepsilon_1)(i2\pi J_1(\kappa_{\perp}\rho))e^{i[-k_{\mathrm{z},1}z-\omega t]} \tag{S14}$$

$$\bar{H}_2^{\mathrm{r}}(\bar{r},t)=\hat{\phi}\int_{-\infty}^{+\infty}d\omega\int_0^{+\infty}d\kappa_{\perp}\,\frac{iq}{\omega\varepsilon_0(2\pi)^3}\,(-\omega\varepsilon_0\varepsilon_{\mathrm{z}})(i2\pi J_1(\kappa_{\perp}\rho))(a_2^{-}e^{-\mathrm{i}k_{\mathrm{z},2}z}+a_2^{+}e^{ik_{\mathrm{z},2}z})\,e^{-i\omega t} \tag{S15}$$

$$\bar{H}_3^{\mathrm{r}}(\bar{r},t)=\hat{\phi}\int_{-\infty}^{+\infty}d\omega\int_0^{+\infty}d\kappa_{\perp}\,\frac{iq}{\omega\varepsilon_0(2\pi)^3}\,a_3(-\omega\varepsilon_0\varepsilon_3)(i2\pi J_1(\kappa_{\perp}\rho))e^{i[+k_{\mathrm{z},3}z-\omega t]} \tag{S16}$$

$$a_{\mathrm{backward}}=a_{1|2}^{-,0}+a_{1|2}^{+,0}\frac{R_{2|3}T_{2|1}}{1-R_{2|3}R_{2|1}e^{i2k_{\mathrm{z},2}d}}e^{i2k_{\mathrm{z},2}d}+a_{2|3}^{-,0}\frac{T_{2|1}}{1-R_{2|3}R_{2|1}e^{i2k_{\mathrm{z},2}d}}e^{i\frac{\omega}{v}d}e^{ik_{\mathrm{z},2}d} \tag{S17}$$

$$a_2^{-}=a_{1|2}^{+,0}\frac{R_{2|3}}{1-R_{2|3}R_{2|1}e^{i2k_{\mathrm{z},2}d}}e^{i2k_{\mathrm{z},2}d}+a_{2|3}^{-,0}\frac{1}{1-R_{2|3}R_{2|1}e^{i2k_{\mathrm{z},2}d}}e^{i\frac{\omega}{v}d}e^{ik_{\mathrm{z},2}d} \tag{S18}$$

$$a_2^{+}=a_{1|2}^{+,0}\frac{1}{1-R_{2|3}R_{2|1}e^{i2k_{\mathrm{z},2}d}}+a_{2|3}^{-,0}\frac{R_{2|1}}{1-R_{2|3}R_{2|1}e^{i2k_{\mathrm{z},2}d}}e^{i\frac{\omega}{v}d}e^{ik_{\mathrm{z},2}d} \tag{S19}$$

$$a_{\mathrm{forward}}=a_{2|3}^{+,0}e^{i\frac{\omega}{v}d}e^{-ik_{\mathrm{z},3}d}+a_{1|2}^{+,0}\frac{T_{2|3}}{1-R_{2|3}R_{2|1}e^{i2k_{\mathrm{z},2}d}}e^{ik_{\mathrm{z},2}d}e^{-ik_{\mathrm{z},3}d}+$$

$$a_{2|3}^{-,0}\frac{R_{2|1}T_{2|3}}{1-R_{2|3}R_{2|1}e^{i2k_{\mathrm{z},2}d}}e^{i\frac{\omega}{v}d}e^{i2k_{\mathrm{z},2}d}e^{-ik_{\mathrm{z},3}d} \tag{S20}$$

$$a_{1|2}^{-,0}=\frac{\kappa_{\perp}^2c^2}{\omega^2}\cdot\frac{-v}{c}\cdot\varepsilon_{\perp}\frac{1}{\varepsilon_1\frac{k_{\mathrm{z},2}}{\omega/c}+\varepsilon_{\perp}\frac{k_{\mathrm{z},1}}{\omega/c}}\left[\frac{1-\frac{v}{c}\frac{k_{\mathrm{z},2}}{\omega/c}}{\varepsilon_{\mathrm{z}}(1-\frac{v^2}{c^2}\varepsilon_{\perp}+\frac{\kappa_{\perp}^2v^2\varepsilon_{\perp}}{\omega^2\ \varepsilon_{\mathrm{z}}})}-\frac{1-\frac{v}{c}\frac{k_{\mathrm{z},2}}{\omega/c}\frac{\varepsilon_{\perp}}{\varepsilon_1}}{\varepsilon_1(1-\frac{v}{c}\frac{k_{\mathrm{z},1}}{\omega/c})(1+\frac{v}{c}\frac{k_{\mathrm{z},1}}{\omega/c})}\right] \tag{S21}$$

$$a_{1|2}^{+,0}=\frac{\kappa_{\perp}^2c^2}{\omega^2}\cdot\frac{+v}{c}\cdot\frac{\varepsilon_1\varepsilon_{\perp}}{\varepsilon_{\mathrm{z}}}\frac{1}{\varepsilon_1\frac{k_{\mathrm{z},2}}{\omega/c}+\varepsilon_{\perp}\frac{k_{\mathrm{z},1}}{\omega/c}}\left[\frac{1+\frac{v}{c}\frac{k_{\mathrm{z},1}}{\omega/c}}{\varepsilon_1(1-\frac{v^2}{c^2}\varepsilon_1+\frac{\kappa_{\perp}^2v^2}{\omega^2})}-\frac{1+\frac{v}{c}\frac{k_{\mathrm{z},1}}{\omega/c}\frac{\varepsilon_{\perp}}{\varepsilon_1}}{\varepsilon_{\mathrm{z}}(1-\frac{v^2}{c^2}\varepsilon_{\perp}+\frac{\kappa_{\perp}^2v^2\varepsilon_{\perp}}{\omega^2\ \varepsilon_{\mathrm{z}}})}\right] \tag{S22}$$

$$a_{2|3}^{-,0}=\frac{\kappa_{\perp}^2c^2}{\omega^2}\cdot\frac{-v}{c}\cdot\frac{\varepsilon_{\perp}\varepsilon_3}{\varepsilon_{\mathrm{z}}}\frac{1}{\varepsilon_{\perp}\frac{k_{\mathrm{z},3}}{\omega/c}+\varepsilon_3\frac{k_{\mathrm{z},2}}{\omega/c}}\left[\frac{1-\frac{v}{c}\frac{k_{\mathrm{z},3}}{\omega/c}}{\varepsilon_3(1-\frac{v^2}{c^2}\varepsilon_3+\frac{\kappa_{\perp}^2v^2}{\omega^2})}-\frac{1-\frac{v}{c}\frac{k_{\mathrm{z},3}}{\omega/c}\frac{\varepsilon_{\perp}}{\varepsilon_3}}{\varepsilon_{\mathrm{z}}(1-\frac{v^2}{c^2}\varepsilon_{\perp}+\frac{\kappa_{\perp}^2v^2\varepsilon_{\perp}}{\omega^2\ \varepsilon_{\mathrm{z}}})}\right] \tag{S23}$$

$$a_{2|3}^{+,0}=\frac{\kappa_{\perp}^2c^2}{\omega^2}\cdot\frac{+v}{c}\cdot\varepsilon_{\perp}\frac{1}{\varepsilon_{\perp}\frac{k_{\mathrm{z},3}}{\omega/c}+\varepsilon_3\frac{k_{\mathrm{z},2}}{\omega/c}}\left[\frac{1+\frac{v}{c}\frac{k_{\mathrm{z},2}}{\omega/c}}{\varepsilon_{\mathrm{z}}(1-\frac{v^2}{c^2}\varepsilon_{\perp}+\frac{\kappa_{\perp}^2v^2\varepsilon_{\perp}}{\omega^2\ \varepsilon_{\mathrm{z}}})}-\frac{1+\frac{v}{c}\frac{k_{\mathrm{z},2}}{\omega/c}\frac{\varepsilon_3}{\varepsilon_{\perp}}}{\varepsilon_3(1-\frac{v}{c}\frac{k_{\mathrm{z},3}}{\omega/c})(1+\frac{v}{c}\frac{k_{\mathrm{z},3}}{\omega/c})}\right] \tag{S24}$$

In the above equations, ω is the angular frequency, t is the time, $\kappa_{\perp}=|\bar{\kappa}_{\perp}|$, ε_0 is the permittivity of free space, and J_1 is the first-order Bessel function. The vectors $\hat{\rho}$, $\hat{\phi}$, and $\hat{z}$ are the unit vectors for the cylindrical coordinate system.

In equation (S10), the total magnetic field $\bar{H}_j(\bar{r},t)$ is separated into two parts, namely $\bar{H}_j^{\mathrm{q}}(\bar{r},t)$ and $\bar{H}_j^{\mathrm{r}}(\bar{r},t)$. To be specific, the charge field $\bar{H}_j^{\mathrm{q}}(\bar{r},t)$ corresponds to the field induced by the electron's motion inside a homogeneous medium; $\bar{H}_j^{\mathrm{r}}(\bar{r},t)=\bar{H}_j(\bar{r},t)-\bar{H}_j^{\mathrm{q}}(\bar{r},t)$ is oftentimes referred to as the radiation field

and appears if the transition radiation occurs. $R_{2|1}$ and $T_{2|1}$ ($R_{2|3}$ and $T_{2|3}$) are the reflection and transmission coefficients at the boundary between region 2 and region 1 (region 3), respectively. To be specific, we have

$$R_{2|1}=\frac{\frac{k_{z,2}}{\varepsilon_\perp}-\frac{k_{z,1}}{\varepsilon_1}}{\frac{k_{z,2}}{\varepsilon_\perp}+\frac{k_{z,1}}{\varepsilon_1}};\ R_{2|3}=\frac{\frac{k_{z,2}}{\varepsilon_\perp}-\frac{k_{z,3}}{\varepsilon_3}}{\frac{k_{z,2}}{\varepsilon_\perp}+\frac{k_{z,3}}{\varepsilon_3}};\ T_{2|1}=\frac{2\frac{k_{z,2}\varepsilon_z}{\varepsilon_\perp\ \varepsilon_1}}{\frac{k_{z,2}}{\varepsilon_\perp}+\frac{k_{z,1}}{\varepsilon_1}};\ T_{2|3}=\frac{2\frac{k_{z,2}\varepsilon_z}{\varepsilon_\perp\ \varepsilon_3}}{\frac{k_{z,2}}{\varepsilon_\perp}+\frac{k_{z,3}}{\varepsilon_3}} \tag{S25}$$

Section S2. Angular spectral energy density and radiation spectrum of transition radiation

To quantitatively discuss the far-field radiation, below we analytically calculate the backward radiation energy W_1 of excited propagating waves, namely the photon energy emitted into region 1. In principle, the backward radiation energy can be obtained by integrating the field energy density over all space in region 1 at $t\to\infty$. At $t\to\infty$, the emitted radiation field, which is a light pulse in the time domain, is already far away from the interface and well separated from the charge field. If we move the coordinate origin along the particle trajectory into the position having the light pulse, the integration with respect to z can be performed from $-\infty$ to $+\infty$, since the field of excited propagating waves is attenuated in both directions away from the central position of the pulse.

For the excited propagating waves in region 1 (namely free space in this work), the electric and magnetic energy densities are equal. This way, the backward radiation energy can be readily expressed as

$$W_1=\int \mathrm{d}x\mathrm{d}y\int_{-\infty}^{+\infty}\mathrm{d}z\cdot\varepsilon_0\varepsilon_1|\bar{E}_1^R(\bar{r},t)|^2 \tag{S26}$$

$$|\bar{E}_1^R(\bar{r},t)|^2=\int \bar{E}_{1|\bar{\kappa}_\perp,\omega}^R(\bar{r},t)\cdot\bar{E}_{1|\bar{\kappa}'_\perp,\omega'}^R(z)e^{i[(\bar{\kappa}_\perp-\bar{\kappa}'_\perp)\cdot\bar{r}_\perp-(\omega-\omega')t]}\,\mathrm{d}\bar{\kappa}_\perp\mathrm{d}\bar{\kappa}'_\perp\mathrm{d}\omega\mathrm{d}\omega' \tag{S27}$$

By substituting equation (S27) into equation (S26) and performing the integration over $\mathrm{d}\bar{\kappa}'_\perp$ and $\mathrm{d}\omega'$, we obtain

$$W_1=2\int_0^{+\infty}\mathrm{d}\omega\int\varepsilon_0\varepsilon_1|a_1|^2\left(\frac{q}{\omega\varepsilon_0(2\pi)^3}\right)^2\frac{\omega^2}{c\kappa_\perp^2}\sqrt{\varepsilon_1}\sqrt{1-\frac{\kappa_\perp^2c^2}{\omega^2\varepsilon_1}}(2\pi)^3\mathrm{d}\bar{\kappa}_\perp \tag{S28}$$

For the excited propagating waves in region 1, we have $\kappa_\perp^2<(\omega^2/c^2)\varepsilon_1$. As such, the integration over $\mathrm{d}\bar{\kappa}_\perp$ in equation (S28) is operated in the range $\kappa_\perp^2<(\omega^2/c^2)\varepsilon_1$. We can further express $\kappa_\perp=(\omega/c)\sqrt{\varepsilon_1}\sin\theta$, by defining θ to be the angle between the wavevector of excited propagating waves and $-\hat{z}$ ($+\hat{z}$) for backward (forward) radiation; see Fig. 3e. Then we have $2\pi\kappa_\perp\mathrm{d}\kappa_\perp=2\pi(\omega^2/c^2)\varepsilon_1\sin\theta\cos\theta\mathrm{d}\theta$. By substituting this relation into equation (S28), we obtain

$$W_1=\int_0^{+\infty}W_1(\omega,v)\,\mathrm{d}\omega \tag{S29}$$

$$W_1(\omega, v) = \int_0^{\pi/2} U_1(\omega, \theta, v) \cdot (2\pi \sin\theta) \mathrm{d}\theta \text{ and } U_1(\omega, \theta, v) = \frac{\varepsilon_1^{3/2} q^2 \cos^2\theta}{4\pi^3 \varepsilon_0 c \sin^2\theta} |a_{\text{backward}}|^2 \quad \text{(S30)}$$

where $W_1(\omega, v)$ and $U_1(\omega, \theta, v) = \frac{\varepsilon_1^{3/2} q^2 \cos^2\theta}{4\pi^3 \varepsilon_0 c \sin^2\theta} |a_{\text{backward}}|^2$ are the radiation spectrum and the angular spectral energy density for the backward radiation.

For the forward radiation, its angular spectral energy density and radiation spectrum can be obtained as $U_3(\omega, \theta, v) = \frac{\varepsilon_3^{3/2} q^2 \cos^2\theta}{4\pi^3 \varepsilon_0 c \sin^2\theta} |a_{\text{forward}}|^2$ and $W_3(\omega, v) = \int_0^{\pi/2} U_3(\omega, \theta, v) \cdot (2\pi \sin\theta) \mathrm{d}\theta$ by following a similar calculation procedure.

Then the total angular spectral energy density of transition radiation can be written as $U(\omega, \theta, v) = U_1(\omega, \theta, v) + U_3(\omega, \theta, v)$, and the total radiation spectrum can be expressed as $W(\omega, v) = W_1(\omega, v) + W_3(\omega, v)$.

More discussion on $k_{z,1}$, $k_{z,2}$, and $k_{z,3}$

The z-components of wavevectors of excited waves in regions 1-3 are defined as $k_{z,1} = \sqrt{\varepsilon_1 \omega^2/c^2 - \kappa_\perp^2}$, $k_{z,2} = \sqrt{\varepsilon_\perp \omega^2/c^2 - \kappa_\perp^2 \varepsilon_\perp/\varepsilon_z}$, and $k_{z,3} = \sqrt{\varepsilon_3 \omega^2/c^2 - \kappa_\perp^2}$, respectively, which are actually multi-value functions and should be rigorously defined during the calculation of the radiation spectra and the angular spectral energy densities. As background, both regions 1 & 3 are lossless vacuum with a relative permittivity of $\varepsilon_1 = \varepsilon_3 = 1$, region 2 is the uniaxial BN with a certain material loss, and this work mainly studies the excited waves that can freely propagate in vacuum. For these excited propagating waves in vaccum, $\kappa_\perp$ is a purely-real and positive value, and we have $0 \le \kappa_\perp \le \omega/c$. Accordingly, both $k_{z,1}$ and $k_{z,3}$ in lossless vacuum are also purely real and positive values. Similarly, the value of $Im(k_{z,2})$ should be positive, for arbitrary ε_z or $\varepsilon_\perp/\varepsilon_z$, to fulfill the radiation condition [63]. That is, $k_{z,2}$ is in the first or second quadrant of the complex $k_{z,2}$ plane for the lossy BN. In addition, the detailed discussion about the choice of the multi-value function of $k_{z,m}$ ($m = 1$, 2, or 3) has been provided in our previous work about Sommerfeld integration in BN-based polaritonic systems [62]; see Fig. 2 in Ref. [62].

Section S3. Discussion on the Sommerfeld integration

The revealed phenomenon of low-velocity-favored transition radiation is not related to the excitation of guided modes (e.g., BN's phonon polaritons). While the electron's penetration through the epsilon-near-zero slab may excite some guided modes, they cannot couple into free space due to the momentum mismatch.

Accordingly, the excited guided modes would not have an impact on the performance of the angular spectral energy densities and radiation spectra of excited propagating waves.

Actually, the revealed phenomenon of low-velocity-favored transition radiation is mainly based on the results of angular spectral energy densities (e.g. Fig. 3a-d) and radiation spectra (e.g. Fig. 2, Fig. 4) of excited propagating waves, whose calculation is irrelevant to the Sommerfeld integration. The Sommerfeld integration is generally used to deal with the integration in the complex wavevector plane with singularity poles, which correspond to the existence of some guided modes (e.g. BN's phonon polaritons). Correspondingly, the Sommerfeld integration is oftentimes used for the numerical calculation of field distribution of excited guided modes in the near field [3,5,59-61]. By contrast, our finding in this work is only related to the emission of propagating waves into the far field, without involving any guided modes and thus the Sommerfeld integration; similarly, the field plot in Fig. 3e-h also aims to show the field distribution of excited propagating waves in the far field.

Section S4. Discussion on the origin of the transition radiation of Ferrell-Berreman modes

Essentially, the underlying mechanism for the transition radiation of Ferrell-Berreman modes (also known as Ferrell radiation) is that the bulk plasmons provide a unique route to extend the electron-interface interaction time, then create light emission far beyond the formation time historically defined for free-electron radiation, and thus help to greatly enhance the radiation intensity [4]. A detailed discussion about this mechanism and a historical survey of Ferrell radiation are provided in a recent work entitled "Bulk-plasmon-mediated free-electron radiation beyond the conventional formation time" [4]. Briefly speaking, this bulk-plasmon-mediated free-electron radiation can occur when a fast-moving electron crosses the interface between free space and a plasmonic medium supporting bulk plasmons, such as metals at the plasma frequency. While emitted continuously from the crossing point on the interface — thus consistent with the features of transition radiation — the extra radiation beyond the conventional formation time is supported by a long tail of bulk plasmons following the electron's trajectory deep into the plasmonic medium [4]. Such a plasmonic tail mixes surface and bulk effects and provides a sustained channel for electron-interface interaction [4].

If the nonlocal response of epsilon-near-zero materials is considered, the Cherenkov radiation of longitudinal waves would also be excited when the electron moves inside the epsilon-near-zero material [4]. However, due to the material loss and their ultra-short wavelength, the excited longitudinal waves cannot

propagate over a long distance or far away from the electron trajectory and then cannot couple into free space. As a result, the consideration of the excited longitudinal waves and the nonlocal response of epsilon-near-zero materials has a minor influence on the radiation spectrum or angular spectral energy density of excited propagating waves [4].

Section S5. Mechanism for the low-velocity-favored transition radiation

We show in Fig. S1 that the revealed phenomenon of low-velocity-favored transition radiation is due to the interference between the excited Ferrell-Berreman modes. To be specific, this revealed phenomenon could occur if a moving electron penetrates through an epsilon-near-zero slab, as shown in Fig. S1a-d. By contrast, this revealed phenomenon would disappear if the electron moves across an interface between an epsilon-near-zero material and free space, as shown in Fig. S1e-h. Note that the excitation of Ferrell-Berreman modes occurs no matter the moving electron penetrates through a single interface in Fig. S1a-d or two parallel interfaces in Fig. S1e-h, due to the existence of epsilon-near-zero materials in both cases. This way, Fig. S1 indicates that the underlying mechanism for the low-velocity-favored transition radiation, including its plateau and dip in Figs. 2b&4b, is due to the interference of the excited Ferrell-Berreman modes, instead of merely the excitation of Ferrell-Berreman modes.

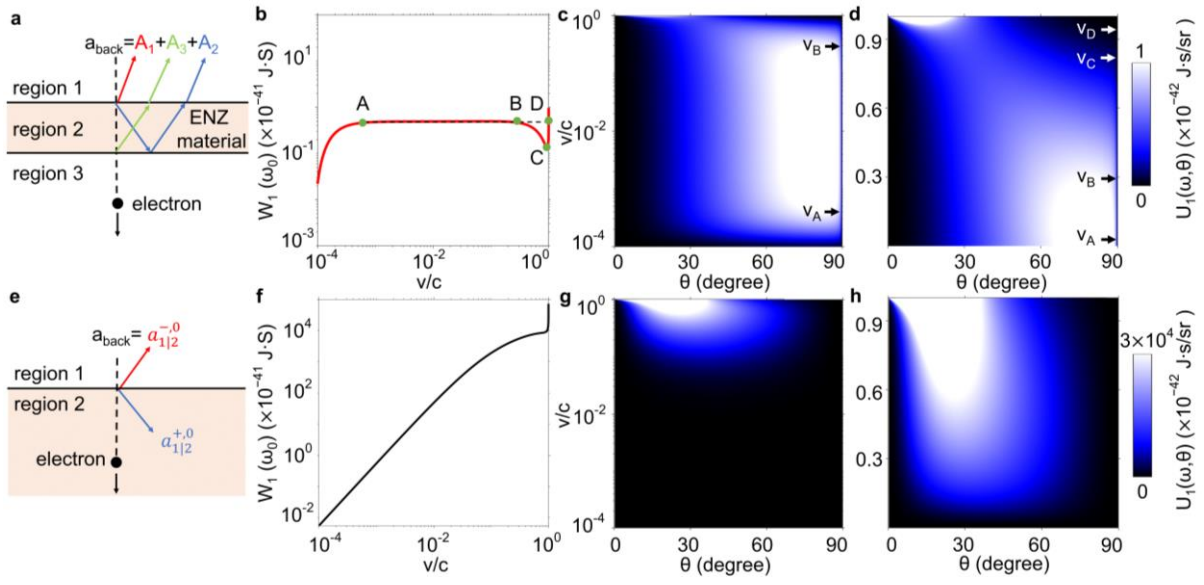

Figure S1. Underlying mechanism for the low-velocity-favored transition radiation. For illustration, here we study two cases of transition radiation. In this figure, region 2 is composed of an epsilon-near-zero material (i.e. BN), while regions 1&3 are both free space. (a-d) Transition radiation induced by the

penetration of moving electrons through an epsilon-near-zero slab. (e-h) Transition radiation induced by the penetration of moving electrons through an interface between free space and an epsilon-near-zero material. The corresponding structural schematics are shown in (a, e). The radiation spectrum of backward radiation, namely $W_1(\omega, v) = \int_0^{\pi/2} U_1(\omega, \theta, v) \cdot (2\pi \sin\theta) \mathrm{d}\theta$, is shown in (b, f). The angular spectral energy density $U_1(\omega, \theta, v)$ of backward radiation in (c, d, g, h) is plotted at the frequency of 24.5 THz, at which we have $\varepsilon_z \to 0$. In order to illustrate the mechanism for the formation of the plateau in Fig. 2b, the y-axes in (c, g) are plotted on a log scale. In order to illustrate the mechanism for the formation of the dip in Fig. 2b, the y-axes in (d, h) are plotted on a linear scale. The angular spectral energy density of backward radiation in region 1 is $U_1(\omega, \theta, v) = \frac{\varepsilon_1^{3/2} q^2 \cos^2\theta}{4\pi^3 \varepsilon_0 c \sin^2\theta} |a_{\mathrm{backward}}|^2$, where the backward radiation coefficient a_{backward} is schematically illustrated in (a, e). To be specific, we have $a_{\mathrm{backward}} = A_1 + A_2 + A_3$ in (a), where $A_1 = a_{1|2}^{-,0}$, $A_2 = a_{1|2}^{+,0} R_{2|3} T_{2|1} / (1 - R_{2|3} R_{2|1} e^{i2k_{z,2}d}) e^{i2k_{z,2}d}$, $A_3 = a_{2|3}^{-,0} T_{2|1} / (1 - R_{2|3} R_{2|1} e^{i2k_{z,2}d}) e^{i\frac{\omega}{v}d} e^{ik_{z,2}d}$; $a_{1|2}^{-,0}$ and $a_{1|2}^{+,0}$ are the backward and forward radiation coefficients if a moving electron penetrates through a single interface between region 1 and region 2; $a_{2|3}^{-,0}$ and $a_{2|3}^{+,0}$ are the backward and forward radiation coefficients if a moving electron penetrates through a single interface between region 2 and region 3; $R_{2|3}$ ($R_{2|1}$) is the reflection coefficient of TM waves between region 2 and region 3 (region 1); $T_{2|1}$ is the transmission coefficient of TM waves between region 2 and region 1. Similarly, we have $a_{\mathrm{backward}} = a_{1|2}^{-,0}$ in Fig. S1e. From Fig. S1a-d, the phenomenon of low-velocity-favored transition radiation occurs, if a moving electron penetrates through an epsilon-near-zero slab. By contrast, from Fig. S1e-h, the phenomenon of low-velocity-favored transition radiation disappears, if the electron moves across an interface between an epsilon-near-zero material and free space. For both cases of transition radiation, the Ferrell-Berreman mode would be excited, due to the existence of epsilon-near-zero materials. It is then reasonable to argue that the occurrence of the low-velocity-favored transition radiation, including its plateau and dip in Fig. 2b, is due to the interference of excited Ferrell-Berreman modes, instead of merely the excitation of Ferrell-Berreman modes.

Mathematical explanation for the emergence of low-velocity-favored transition radiation

The limit of radiation spectrum $W(\omega, v)$ can be analytically obtained under the conditions of $\varepsilon_z(\omega) \to 0$, $\omega d/c \ll \sqrt{|\varepsilon_z/\varepsilon_\perp|}$, and $\omega d/c \ll v/c \ll 1$; see details below. When these conditions are fulfilled, the radiation spectrum becomes irrelevant to the electron velocity v as shown in Figs. S2-S3. This exactly corresponds to the revealed phenomenon of low-velocity-favored transition radiation from an ultrathin epsilon-near-zero slab, which is featured with a plateau of largely-enhanced radiation spectrum in a certain range of electron velocity. Moreover, since the condition of $\omega d/c \ll v/c \ll 1$ is sensitive to the slab thickness d, the velocity range within which the low-velocity-favored transition radiation could occur is also highly dependent on the slab thickness as shown in Fig. S2.

We now proceed to derive the limit of radiation spectrum $W(\omega, v)$. According to the definition of radiation spectrum in section S2, we have $W(\omega, v) = \int_0^{\pi/2} U_1(\omega, \theta, v) \cdot (2\pi\sin\theta)\mathrm{d}\theta + \int_0^{\pi/2} U_3(\omega, \theta, v) \cdot (2\pi\sin\theta)\mathrm{d}\theta$, where the backward angular spectral energy density is $U_1(\omega, \theta, v) = \frac{\varepsilon_1^{3/2} q^2 \cos^2\theta}{4\pi^3 \varepsilon_0 c \sin^2\theta} |a_{\mathrm{backward}}|^2$, and the forward angular spectral energy density is $U_3(\omega, \theta, v) = \frac{\varepsilon_3^{3/2} q^2 \cos^2\theta}{4\pi^3 \varepsilon_0 c \sin^2\theta} |a_{\mathrm{forward}}|^2$. That is, the radiation spectrum is determined by the backward radiation coefficient a_{backward} and the forward radiation coefficient a_{forward}. To facilitate the understanding of the radiation spectrum, we firstly derive the limit of a_{backward}. According to equation (S17), we have $a_{\mathrm{backward}} = a_{1|2}^{-,0} + a_{1|2}^{+,0} \frac{R_{2|3} T_{2|1}}{1 - R_{2|3} R_{2|1} e^{i2k_{z,2}d}} e^{i2k_{z,2}d} + a_{2|3}^{-,0} \frac{T_{2|1}}{1 - R_{2|3} R_{2|1} e^{i2k_{z,2}d}} e^{i\frac{\omega}{v}d} e^{ik_{z,2}d}$, where $\varepsilon_3 = \varepsilon_1$ is used in this work, $T_{2|1} = 2\frac{k_{z,2}}{\varepsilon_\perp} \cdot \frac{\varepsilon_z}{\varepsilon_1} / (\frac{k_{z,2}}{\varepsilon_\perp} + \frac{k_{z,1}}{\varepsilon_1})$ is the transmission coefficient, and $R_{2|1} = R_{2|3} = (\frac{k_{z,2}}{\varepsilon_\perp} - \frac{k_{z,1}}{\varepsilon_1}) / (\frac{k_{z,2}}{\varepsilon_\perp} + \frac{k_{z,1}}{\varepsilon_1})$ is the reflection coefficient. If $v/c \ll 1$ and $\varepsilon_z \ll 1$, according to equations (S21-S23), we approximately have $a_{1|2}^{-,0} = \frac{\kappa_\perp^2 c^2}{\omega^2} \cdot \frac{-v}{c} \cdot \varepsilon_\perp \frac{1}{\varepsilon_1 \frac{k_{z,2}}{\omega/c} + \varepsilon_\perp \frac{k_{z,1}}{\omega/c}} \frac{1 - \frac{v}{c}\frac{k_{z,2}}{\omega/c}}{\varepsilon_z (1 - \frac{v^2}{c^2}\varepsilon_\perp + \frac{\kappa_\perp^2 v^2 \varepsilon_\perp}{\omega^2 \varepsilon_z})}$, $a_{1|2}^{+,0} = \frac{\kappa_\perp^2 c^2}{\omega^2} \cdot \frac{+v}{c} \cdot \varepsilon_\perp \frac{\varepsilon_1}{\varepsilon_z} \frac{1}{\varepsilon_1 \frac{k_{z,2}}{\omega/c} + \varepsilon_\perp \frac{k_{z,1}}{\omega/c}} [-\frac{1 + \frac{v}{c}\frac{k_{z,1}}{\omega/c}\frac{\varepsilon_\perp}{\varepsilon_1}}{\varepsilon_z (1 - \frac{v^2}{c^2}\varepsilon_\perp + \frac{\kappa_\perp^2 v^2 \varepsilon_\perp}{\omega^2 \varepsilon_z})}]$, and $a_{2|3}^{-,0} = \frac{\kappa_\perp^2 c^2}{\omega^2} \cdot \frac{-v}{c} \cdot \varepsilon_\perp \frac{\varepsilon_1}{\varepsilon_z} \frac{1}{\varepsilon_\perp \frac{k_{z,3}}{\omega/c} + \varepsilon_3 \frac{k_{z,2}}{\omega/c}} [-\frac{1 - \frac{v}{c}\frac{k_{z,1}}{\omega/c}\frac{\varepsilon_\perp}{\varepsilon_1}}{\varepsilon_z (1 - \frac{v^2}{c^2}\varepsilon_\perp + \frac{\kappa_\perp^2 v^2 \varepsilon_\perp}{\omega^2 \varepsilon_z})}]$. Moreover, if the condition of $v^2/c^2 \ll |\varepsilon_z/\varepsilon_\perp|$ is fulfilled, we then approximately have $a_{1|2}^{-,0} = \frac{\kappa_\perp^2 c^2}{\omega^2} \cdot \frac{-v}{c} \cdot \frac{\omega/c}{\frac{k_{z,2}}{\varepsilon_\perp} + \frac{k_{z,1}}{\varepsilon_1}} \frac{1}{\varepsilon_1 \varepsilon_z}$; since $|\varepsilon_z| \ll |\varepsilon_\perp|$ in this work, this expression can

be further simplified to $a_{1|2}^{-,0}=\frac{k_{z,2}v}{\omega\varepsilon_1}$; under these additional conditions, we also have $a_{1|2}^{+,0}=-a_{2|3}^{-,0}=a_{1|2}^{-,0}\frac{\varepsilon_1}{\varepsilon_z}$. While the additional condition of $v^2/c^2 \ll |\varepsilon_z/\varepsilon_\perp|$ is very helpful for the simplification of $a_{1|2}^{-,0}$, $a_{1|2}^{+,0}$, and $a_{2|3}^{-,0}$, there is actually no necessity to use this condition for the simplification of a_{backward}; see detailed derivation in below subsection entitled "Derivation of the simplified expression for a_{backward} in equation (S31) without the assumption of $v^2/c^2 \ll |\varepsilon_z/\varepsilon_\perp|$". In short, after some calculations without the assumption of $v^2/c^2 \ll |\varepsilon_z/\varepsilon_\perp|$, the backward radiation coefficient can be further approximately reduced to

$$a_{\text{backward}}=i\kappa_\perp^2\cdot\frac{1}{\frac{2k_{z,1}}{\varepsilon_1}-\frac{ik_{z,2}\cdot dk_{z,2}}{\varepsilon_\perp}}\frac{d}{\varepsilon_1\varepsilon_z}=\frac{1}{\varepsilon_1-2i\frac{k_{z,1}}{k_\perp}\cdot\frac{\varepsilon_z}{k_\perp d}} \tag{S31}$$

Similarly, under the conditions of $\varepsilon_z(\omega)\to 0$, $\omega d/c \ll \sqrt{|\varepsilon_z/\varepsilon_\perp|}$, and $\omega d/c \ll v/c \ll 1$, the forward radiation coefficient can be approximately reduced to

$$a_{\text{forward}}=i\kappa_\perp^2\cdot\frac{1}{\frac{2k_{z,1}}{\varepsilon_1}-\frac{ik_{z,2}\cdot dk_{z,2}}{\varepsilon_\perp}}\frac{d}{\varepsilon_1\varepsilon_z}=\frac{1}{\varepsilon_1-2i\frac{k_{z,1}}{k_\perp}\cdot\frac{\varepsilon_z}{k_\perp d}} \tag{S32}$$

Since both the backward and forward radiation coefficients in equations (S31-S32) are independent of the electron velocity and almost linearly proportional to $1/\varepsilon_z$, the radiation spectrum $W(\omega,v)$ is then also irrelevant to the electron velocity and almost linearly proportional to $1/|\varepsilon_z|^2$. We show in Figs. S2-S3 that the radiation spectra with and without the above approximation match well within the range of $\omega d/c \ll v/c \ll 1$, if $\varepsilon_z(\omega)\to 0$ and $\omega d/c \ll \sqrt{|\varepsilon_z/\varepsilon_\perp|}$. Therefore, if the conditions of $\varepsilon_z(\omega)\to 0$, $\omega d/c \ll \sqrt{|\varepsilon_z/\varepsilon_\perp|}$, and $\omega d/c \ll v/c \ll 1$ are fulfilled, the revealed phenomenon of low-velocity-favored transition radiation could occur.

In addition, we note that the Ferrell radiation (or one specific peak observed in the transition-radiation spectrum) is closely related to the reflection coefficient, as pointed out by Economou in 1969 [*Phys. Rev.* **182**, 539 (1969)]. While our revealed phenomenon of low-velocity-favored transition radiation is related to the Ferrell radiation, its origin is not determined by the reflection coefficient. This can be seen from equations (S31-S32), in which the backward and forward radiation coefficients are not relevant to the reflection coefficient. Actually, the reflection coefficient itself is a physical parameter which is dependent on the frequency and the incident angle but not related to the electron velocity, and it thus cannot explain the dependence of our revealed phenomenon on the electron velocity.

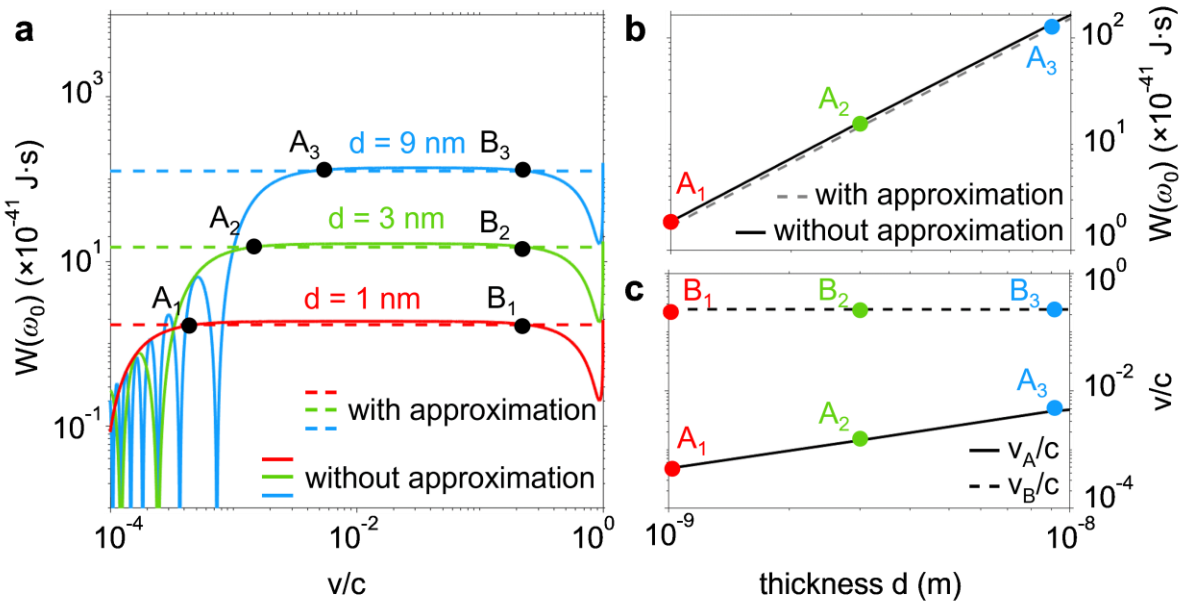

Figure S2. Influence of the slab thickness d on the low-velocity-favored transition radiation. For illustration, the epsilon-near-zero slab here is set to have a relative permittivity of $[\varepsilon_\perp, \varepsilon_\perp, \varepsilon_z] = [7.7, 7.7, -0.05]$ and a thickness of 1 nm, 3 nm, or 9 nm. The other structural setup is the same as Fig. 2. (a) Radiation spectrum $W(\omega_0)$ of the excited propagating waves as a function of the electron velocity v at the frequency of $\omega_0/2\pi = 24.5$ THz for various slab thicknesses. The solid lines are plotted by using the backward radiation coefficients a_{backward} and a_{forward} without any approximation, while the dashed lines are plotted by using a_{backward} in equation (S31) and a_{forward} in equation (S32) with some approximations (i.e., under the assumption of $\varepsilon_z \to 0$, $\omega d/c \ll \sqrt{|\varepsilon_z/\varepsilon_\perp|}$ and $\omega d/c \ll v/c \ll 1$). When the slab thickness increases, the velocity range that possesses the phenomenon of low-velocity-favored transition radiation would become narrower. (b) Dependence of $W(\omega_0)$ on the slab thickness when $v = v_A$, as extracted from (a). (c) Dependence of v_A (solid line) and v_B (dashed line) on the slab thickness, as extracted from (a). The value of v_A would increase if the slab thickness increases, while the value of v_B is relatively insensitive to the variation of the slab thickness.

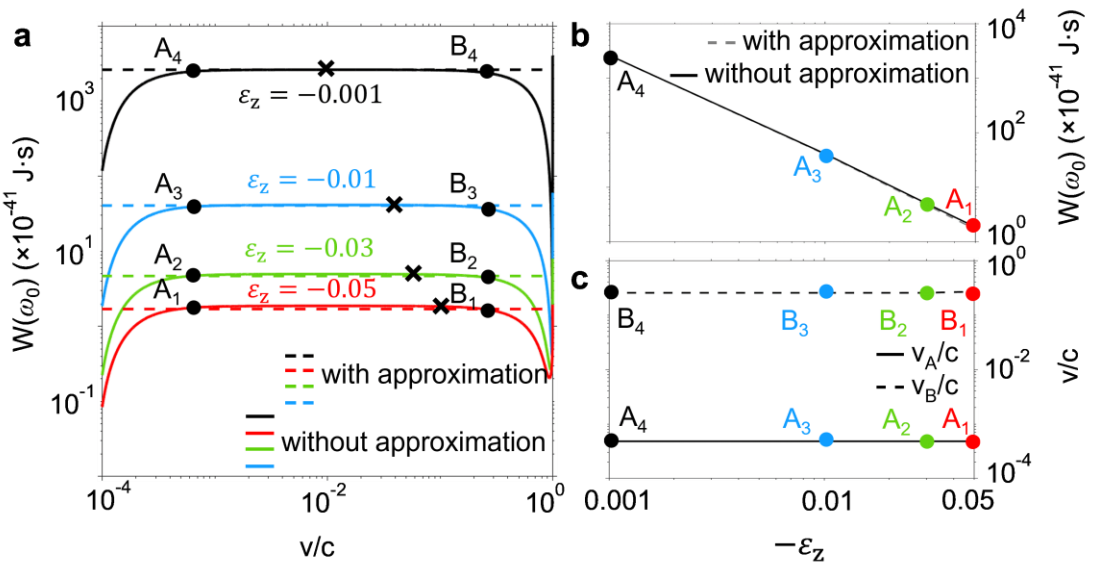

Figure S3. Influence of ε_z on the low-velocity-favored transition radiation. For illustration, the epsilon-near-zero slab here is set to have a thickness of 1 nm and a relative permittivity of $[\varepsilon_\perp, \varepsilon_\perp, \varepsilon_z] = [7.7, 7.7, \varepsilon_z]$, where ε_z is equal to -0.001, -0.01, -0.03, or -0.05 in this figure. The other structural setup is the same as Fig. S2. (a) Radiation spectrum $W(\omega_0)$ of the excited propagating waves as a function of the electron velocity v at the frequency of $\omega_0/2\pi = 24.5$ THz for various values of ε_z. The solid lines are plotted by using the backward radiation coefficients a_{backward} and a_{forward} without any approximation, while the dashed lines are plotted by using a_{backward} in equation (S31) and a_{forward} in equation (S32) with some approximations (i.e., under the assumption of $\varepsilon_z \to 0$, $\omega d/c \ll \sqrt{|\varepsilon_z/\varepsilon_\perp|}$ and $\omega d/c \ll v/c \ll 1$). For comparison, the position of $v/c = \sqrt{|\varepsilon_z/\varepsilon_\perp|}$ is denoted by the cross marker for each line. (b) Dependence of $W(\omega_0)$ on the slab thickness when $v = v_A$, as extracted from (a). (c) Dependence of v_A (solid line) and v_B (dashed line) on $-\varepsilon_z$, as extracted from (a). For illustration, the value of $W(\omega_0)$ at $v = v_A$ or $v = v_B$ is defined to be 90% of the maximum within the range of $v \in [v_A, v_B]$. Both of the values of v_A and v_B are relatively insensitive to the variation of $|\varepsilon_z|$.

Derivation of the simplified expression for a_{backward} in equation (S31) without the assumption of $v^2/c^2 \ll |\varepsilon_z/\varepsilon_\perp|$

Despite the condition of $v^2/c^2 \ll |\varepsilon_z/\varepsilon_\perp|$ is helpful for the simplification of the factor $1 - \frac{v^2}{c^2}\varepsilon_\perp + \frac{\kappa_\perp^2 v^2}{\omega^2}\frac{\varepsilon_\perp}{\varepsilon_z}$ in all $a_{1|2}^{+,0}$, $a_{1|2}^{-,0}$ and $a_{2|3}^{-,0}$, there is actually no necessity to assume this condition for the simplification of

a_{backward}. The underlying reason is that a_{backward} in equation (S17) is a summation related to $a_{1|2}^{+,0}$, $a_{1|2}^{-,0}$ and $a_{2|3}^{-,0}$, and the key factor $1-\frac{v^2}{c^2}\varepsilon_\perp+\frac{\kappa_1^2 v^2}{\omega^2}\frac{\varepsilon_\perp}{\varepsilon_z}$ in all $a_{1|2}^{+,0}$, $a_{1|2}^{-,0}$ and $a_{2|3}^{-,0}$ could be cancelled out automatically during their summation without the assumption of the mentioned condition of $v^2/c^2 \ll |\varepsilon_z/\varepsilon_\perp|$; see detailed derivation below. That is, the condition of $v^2/c^2 \ll |\varepsilon_z/\varepsilon_\perp|$ is not a necessary condition to achieve the simplified expression for a_{backward} in our equation (S31), and it thus could not define the position of point B in all related figures (e.g. Figs. S2-S3). This happens even when we consider the case of $\varepsilon_z=-0.001$ in Fig. S3. From Fig. S3, on the one hand, the value of $v/c=\sqrt{|\varepsilon_z/\varepsilon_\perp|}$ is much smaller than $v/c=v_B/c$; on the other hand, while the value of $v/c=\sqrt{|\varepsilon_z/\varepsilon_\perp|}$ is sensitive to the variation of ε_z, the value of v_B/c (namely the position of point B) is relatively insensitive to the variation of ε_z.

Below we provide the detailed derivation of the simplified expression for a_{backward} in equation (S31) without the assumption of $v^2/c^2 \ll |\varepsilon_z/\varepsilon_\perp|$.

For the ultrathin epsilon-near-zero slab considered in this work, if $|\varepsilon_z| \ll 1$ and $\omega d/c \ll \sqrt{|\varepsilon_z/\varepsilon_\perp|}$, we approximately have $|k_{z,2}d|=\left|\sqrt{\frac{\omega^2}{c^2}\varepsilon_\perp-\kappa_\perp^2\frac{\varepsilon_\perp}{\varepsilon_z}}\right|d=\left|i\kappa_\perp\sqrt{\frac{\varepsilon_\perp}{\varepsilon_z}}\right|d<|\frac{\omega}{c}\sqrt{\frac{\varepsilon_\perp}{\varepsilon_z}}|d\ll 1$ and $e^{ik_{z,2}d}=1+ik_{z,2}d$.

Since the considered structure is also symmetric (i.e. $\varepsilon_1=\varepsilon_3$), we further have $\frac{T_{2|1}e^{ik_{z,2}d}}{1-R_{2|3}R_{2|1}e^{i2k_{z,2}d}}=\frac{T_{2|1}e^{ik_{z,2}d}}{(1-R_{2|1}e^{ik_{z,2}d})(1+R_{2|1}e^{ik_{z,2}d})}=\frac{T_{2|1}}{(1-R_{2|1}e^{ik_{z,2}d})(1+R_{2|1})}=\frac{\varepsilon_z/\varepsilon_1}{1-R_{2|1}e^{ik_{z,2}d}}$. Then the expression of a_{backward} in equation (S17) can be re-organized into

$$a_{\mathrm{backward}}=a_{1|2}^{-,0}+a_{1|2}^{+,0}\frac{\varepsilon_z/\varepsilon_1}{1-R_{2|1}e^{ik_{z,2}d}}R_{2|3}e^{ik_{z,2}d}+a_{2|3}^{-,0}\frac{\varepsilon_z/\varepsilon_1}{1-R_{2|1}e^{ik_{z,2}d}}e^{i\frac{\omega}{v}d} \tag{S33}$$

If $v/c \ll 1$ and $|\varepsilon_z| \ll 1$, we have $|\frac{1-\frac{v}{c}\frac{k_{z,2}}{\omega/c}}{\varepsilon_z\left(1-\frac{v^2}{c^2}\varepsilon_\perp+\frac{\kappa_1^2v^2\varepsilon_\perp}{\omega^2\ \varepsilon_z}\right)}| \gg |\frac{1-\frac{v}{c}\frac{k_{z,2}}{\omega/c}\frac{\varepsilon_1}{\varepsilon_\perp}}{\varepsilon_1\left(1-\frac{v}{c}\frac{k_{z,1}}{\omega/c}\right)\left(1+\frac{v}{c}\frac{k_{z,1}}{\omega/c}\right)}|$. By using this fact for the simplification of $a_{1|2}^{-,0}$, $a_{1|2}^{+,0}$ and $a_{2|3}^{-,0}$ in equations (S21-S23), we approximately have

$$a_{1|2}^{-,0}=\frac{\kappa_1^2c^2}{\omega^2}\cdot\frac{-v}{c}\cdot\varepsilon_\perp\frac{1}{\varepsilon_1\frac{k_{z,2}}{\omega/c}+\varepsilon_\perp\frac{k_{z,1}}{\omega/c}}\frac{1-\frac{v}{c}\frac{k_{z,2}}{\omega/c}}{\varepsilon_z(1-\frac{v^2}{c^2}\varepsilon_\perp+\frac{\kappa_1^2v^2\varepsilon_\perp}{\omega^2\ \varepsilon_z})} \tag{S34}$$

$$a_{1|2}^{+,0}=\frac{\kappa_1^2c^2}{\omega^2}\cdot\frac{+v}{c}\cdot\varepsilon_\perp\frac{\varepsilon_1}{\varepsilon_z}\frac{1}{\varepsilon_1\frac{k_{z,2}}{\omega/c}+\varepsilon_\perp\frac{k_{z,1}}{\omega/c}}\left[-\frac{1+\frac{v}{c}\frac{k_{z,1}}{\omega/c}\frac{\varepsilon_\perp}{\varepsilon_1}}{\varepsilon_z(1-\frac{v^2}{c^2}\varepsilon_\perp+\frac{\kappa_1^2v^2\varepsilon_\perp}{\omega^2\ \varepsilon_z})}\right] \tag{S35}$$

$$a_{2|3}^{-,0} = \frac{\kappa_\perp^2 c^2}{\omega^2} \cdot \frac{-v}{c} \cdot \varepsilon_\perp \frac{\varepsilon_1}{\varepsilon_z} \frac{1}{\varepsilon_\perp \frac{k_{z,3}}{\omega/c} + \varepsilon_3 \frac{k_{z,2}}{\omega/c}} \left[- \frac{1 - \frac{v}{c} \frac{k_{z,1}}{\omega/c} \frac{\varepsilon_\perp}{\varepsilon_1}}{\varepsilon_z \left(1 - \frac{v^2}{c^2}\varepsilon_\perp + \frac{\kappa_\perp^2 v^2}{\omega^2} \frac{\varepsilon_\perp}{\varepsilon_z}\right)} \right] \tag{S36}$$

In equations (S34-S36), each equation has a same factor $1 - \frac{v^2}{c^2}\varepsilon_\perp + \frac{\kappa_\perp^2 v^2}{\omega^2}\frac{\varepsilon_\perp}{\varepsilon_z}$. This factor can be further simplified if the condition of $v^2/c^2 \ll |\varepsilon_z/\varepsilon_\perp|$ is satisfied, and we have $1 - \frac{v^2}{c^2}\varepsilon_\perp + \frac{\kappa_\perp^2 v^2}{\omega^2}\frac{\varepsilon_\perp}{\varepsilon_z} \to 1$. In other words, the usage of the condition of $v^2/c^2 \ll |\varepsilon_z/\varepsilon_\perp|$ is beneficial for the further simplification of $a_{1|2}^{-,0}$, $a_{1|2}^{+,0}$ and $a_{2|3}^{-,0}$ in equations (S34-S36). However, we emphasize that the condition of $v^2/c^2 \ll |\varepsilon_z/\varepsilon_\perp|$ is not necessary for the simplification of a_{backward} in equation (S33). Below, we proceed with the simplification of a_{backward} without the assumption of $v^2/c^2 \ll |\varepsilon_z/\varepsilon_\perp|$.

By substituting equation (S34-S36) directly into equation (S33), we have

$$a_{\text{backward}} = \frac{\kappa_\perp^2 c^2}{\omega^2} \cdot \frac{-v}{c} \cdot \varepsilon_\perp \frac{1}{\varepsilon_1 \frac{k_{z,2}}{\omega/c} + \varepsilon_\perp \frac{k_{z,1}}{\omega/c}} \frac{1 - \frac{v}{c}\frac{k_{z,2}}{\omega/c}}{\varepsilon_z \left(1 - \frac{v^2}{c^2}\varepsilon_\perp + \frac{\kappa_\perp^2 v^2}{\omega^2}\frac{\varepsilon_\perp}{\varepsilon_z}\right)} + \frac{\kappa_\perp^2 c^2}{\omega^2} \cdot \frac{+v}{c} \cdot$$

$$\varepsilon_\perp \frac{-1}{\varepsilon_1 \frac{k_{z,2}}{\omega/c} + \varepsilon_\perp \frac{k_{z,1}}{\omega/c}} \frac{1 + \frac{v}{c}\frac{k_{z,1}}{\omega/c}\frac{\varepsilon_\perp}{\varepsilon_1}}{\varepsilon_z \left(1 - \frac{v^2}{c^2}\varepsilon_\perp + \frac{\kappa_\perp^2 v^2}{\omega^2}\frac{\varepsilon_\perp}{\varepsilon_z}\right)} \frac{R_{2|3} e^{ik_{z,2}d}}{1 - R_{2|1} e^{ik_{z,2}d}} + \frac{\kappa_\perp^2 c^2}{\omega^2} \cdot \frac{-v}{c} \cdot \varepsilon_\perp \frac{-1}{\varepsilon_\perp \frac{k_{z,3}}{\omega/c} + \varepsilon_3 \frac{k_{z,2}}{\omega/c}} \frac{1 - \frac{v}{c}\frac{k_{z,3}}{\omega/c}\frac{\varepsilon_\perp}{\varepsilon_3}}{\varepsilon_z \left(1 - \frac{v^2}{c^2}\varepsilon_\perp + \frac{\kappa_\perp^2 v^2}{\omega^2}\frac{\varepsilon_\perp}{\varepsilon_z}\right)} \frac{e^{i\frac{\omega}{v}d}}{1 - R_{2|1} e^{ik_{z,2}d}}$$

$$= \frac{\kappa_\perp^2 c^2}{\omega^2} \cdot \frac{-v}{c} \cdot \varepsilon_\perp \frac{1}{\varepsilon_1 \frac{k_{z,2}}{\omega/c} + \varepsilon_\perp \frac{k_{z,1}}{\omega/c}} \frac{1}{\varepsilon_z \left(1 - \frac{v^2}{c^2}\varepsilon_\perp + \frac{\kappa_\perp^2 v^2}{\omega^2}\frac{\varepsilon_\perp}{\varepsilon_z}\right)} \left(1 - \frac{v}{c} \cdot \frac{k_{z,2}}{\omega/c} + \frac{R_{2|3} e^{ik_{z,2}d}\left(1 + \frac{v}{c}\frac{k_{z,1}}{\omega/c}\frac{\varepsilon_\perp}{\varepsilon_1}\right) - e^{i\frac{\omega}{v}d}\left(1 - \frac{v}{c}\frac{k_{z,1}}{\omega/c}\frac{\varepsilon_\perp}{\varepsilon_1}\right)}{1 - R_{2|1} e^{ik_{z,2}d}}\right) \tag{S37}$$

As background, we have $R_{2|3} = \frac{\frac{k_{z,2}}{\varepsilon_\perp} - \frac{k_{z,1}}{\varepsilon_1}}{\frac{k_{z,2}}{\varepsilon_\perp} + \frac{k_{z,1}}{\varepsilon_1}} = 1 - 2\frac{k_{z,1}\varepsilon_\perp}{\varepsilon_1 k_{z,2}}$ in equation (S37), and the factor $2\frac{k_{z,1}\varepsilon_\perp}{\varepsilon_1 k_{z,2}} = 2\frac{k_{z,1}\varepsilon_\perp}{\varepsilon_1 \sqrt{\frac{\omega^2}{c^2}\varepsilon_\perp - \kappa_\perp^2 \frac{\varepsilon_\perp}{\varepsilon_z}}} = 2\frac{k_{z,1}\varepsilon_\perp}{\varepsilon_1 i\kappa_\perp \sqrt{\frac{\varepsilon_\perp}{\varepsilon_z}}} = 2\frac{k_{z,1}\sqrt{\varepsilon_\perp}}{i\varepsilon_1 \kappa_\perp}\sqrt{\varepsilon_z}$ could be a small quantity if $|\varepsilon_z| \ll 1$. By only keeping the small quantities up to the first order, then the term $1 - R_{2|1}e^{ik_{z,2}d}$ in equation (S37) can be approximately simplified to

$$1 - R_{2|1} e^{ik_{z,2}d} = 1 - \left(1 - 2\frac{k_{z,1}\varepsilon_\perp}{\varepsilon_1 k_{z,2}}\right)\left(1 + ik_{z,2}d\right) = 2\frac{k_{z,1}\varepsilon_\perp}{\varepsilon_1 k_{z,2}} - ik_{z,2}d \tag{S38}$$

If $\frac{\omega}{v}d \ll 1$ (i.e., $\frac{v}{c} \gg \frac{\omega}{c}d$), we further approximately have $e^{i\frac{\omega}{v}d} = 1 + i\frac{\omega}{v}d$. By only keeping the small quantities up to the first order, then the term $R_{2|3}e^{ik_{z,2}d}\left(1 + \frac{v}{c} \cdot \frac{k_{z,1}}{\omega/c} \cdot \frac{\varepsilon_\perp}{\varepsilon_1}\right) - e^{i\frac{\omega}{v}d}\left(1 - \frac{v}{c} \cdot \frac{k_{z,1}}{\omega/c} \cdot \frac{\varepsilon_\perp}{\varepsilon_1}\right)$ in equation (S37) can be approximately simplified to

$$R_{2|3}e^{ik_{z,2}d}\left(1+\frac{v}{c}\cdot\frac{k_{z,1}}{\omega/c}\cdot\frac{\varepsilon_\perp}{\varepsilon_1}\right)-e^{i\frac{\omega}{v}d}\left(1-\frac{v}{c}\cdot\frac{k_{z,1}}{\omega/c}\cdot\frac{\varepsilon_\perp}{\varepsilon_1}\right)$$

$$=\left(1-2\frac{k_{z,1}\varepsilon_\perp}{\varepsilon_1 k_{z,2}}\right)\left(1+ik_{z,2}d\right)\left(1+\frac{v}{c}\cdot\frac{k_{z,1}}{\omega/c}\cdot\frac{\varepsilon_\perp}{\varepsilon_1}\right)-\left(1+i\frac{\omega}{v}d\right)\left(1-\frac{v}{c}\cdot\frac{k_{z,1}}{\omega/c}\cdot\frac{\varepsilon_\perp}{\varepsilon_1}\right)$$

$$=-2\frac{k_{z,1}}{k_{z,2}}\cdot\frac{\varepsilon_\perp}{\varepsilon_1}\left(1-\frac{v}{c}\cdot\frac{k_{z,2}}{\omega/c}\right)-i\frac{\omega}{v}d+ik_{z,2}d \tag{S39}$$

By substituting equations (S38-S39) into equation (S37), we have

$$a_{\text{backward}}=\frac{\kappa_\perp^2c^2}{\omega^2}\cdot\frac{-v}{c}\cdot\varepsilon_\perp\frac{1}{\varepsilon_1\frac{k_{z,2}}{\omega/c}+\varepsilon_\perp\frac{k_{z,1}}{\omega/c}}\frac{1}{\varepsilon_z\left(1-\frac{v^2}{c^2}\varepsilon_\perp+\frac{\kappa_\perp^2v^2\varepsilon_\perp}{\omega^2\ \varepsilon_z}\right)}\left(1-\frac{v}{c}\cdot\frac{k_{z,2}}{\omega/c}+\frac{-2\frac{k_{z,1}}{k_{z,2}}\frac{\varepsilon_\perp}{\varepsilon_1}\left(1-\frac{v}{c}\frac{k_{z,2}}{\omega/c}\right)-i\frac{\omega}{v}d+ik_{z,2}d}{2\frac{k_{z,1}\varepsilon_\perp}{\varepsilon_1k_{z,2}}-ik_{z,2}d}\right)$$

$$=\frac{\kappa_\perp^2c^2}{\omega^2}\cdot\frac{-v}{c}\cdot\varepsilon_\perp\frac{1}{\varepsilon_1\frac{k_{z,2}}{\omega/c}+\varepsilon_\perp\frac{k_{z,1}}{\omega/c}}\frac{1}{\varepsilon_z(1-\frac{v^2}{c^2}\varepsilon_\perp+\frac{\kappa_\perp^2v^2\varepsilon_\perp}{\omega^2\ \varepsilon_z})}\frac{-i\frac{\omega}{v}d\left(1-(\frac{v}{\omega}k_{z,2})^2\right)}{2\frac{k_{z,1}\varepsilon_\perp}{\varepsilon_1k_{z,2}}-ik_{z,2}d}$$

$$=\frac{\kappa_\perp^2c^2}{\omega^2}\cdot\frac{-v}{c}\cdot\varepsilon_\perp\frac{1}{\varepsilon_1\frac{k_{z,2}}{\omega/c}+\varepsilon_\perp\frac{k_{z,1}}{\omega/c}}\frac{1}{\varepsilon_z(1-\frac{v^2}{c^2}\varepsilon_\perp+\frac{\kappa_\perp^2v^2\varepsilon_\perp}{\omega^2\ \varepsilon_z})}\frac{-i\frac{\omega}{v}d\left(1-\frac{v^2}{c^2}\varepsilon_\perp+\frac{\kappa_\perp^2v^2\varepsilon_\perp}{\omega^2\ \varepsilon_z}\right)}{2\frac{k_{z,1}\varepsilon_\perp}{\varepsilon_1k_{z,2}}-ik_{z,2}d}$$

$$=\frac{\kappa_\perp^2c^2}{\omega^2}\cdot\varepsilon_\perp\frac{1}{\varepsilon_1\frac{k_{z,2}}{\omega/c}+\varepsilon_\perp\frac{k_{z,1}}{\omega/c}}\frac{1}{\varepsilon_z}\frac{i\frac{\omega}{c}d}{2\frac{k_{z,1}\varepsilon_\perp}{\varepsilon_1k_{z,2}}-ik_{z,2}d} \tag{S40}$$

Since $|\varepsilon_z|\ll|\varepsilon_\perp|$ in this work, we approximately have $\left|k_{z,2}\right|=|i\kappa_\perp\sqrt{\frac{\varepsilon_\perp}{\varepsilon_z}}|\gg|k_{z,1}|$ and then $\frac{1}{\varepsilon_1\frac{k_{z,2}}{\omega/c}+\varepsilon_\perp\frac{k_{z,1}}{\omega/c}}=\frac{1}{\varepsilon_1\frac{k_{z,2}}{\omega/c}}$. This way, equation (S40) can be further simplified to

$$a_{\text{backward}}=i\kappa_\perp^2\cdot\frac{1}{\frac{2k_{z,1}}{\varepsilon_1}-\frac{ik_{z,2}\cdot dk_{z,2}}{\varepsilon_\perp}}\frac{d}{\varepsilon_1\varepsilon_z}=\frac{1}{\varepsilon_1-2i\frac{k_{z,1}}{k_\perp}\frac{\varepsilon_z}{k_\perp d}} \tag{S41}$$

Note that equation (S41) is exactly the simplified expression for a_{backward} in equation (S31). By following a similar calculation procedure, the simplified expression for a_{forward} in equation (S32) can also be derived without the assumption of $v^2/c^2\ll|\varepsilon_z/\varepsilon_\perp|$.

According to the above derivation, the necessary conditions to obtain the simplified expression for a_{backward} in equation (S31) are $|\varepsilon_z|\to0$, $\omega d/c\ll\sqrt{|\varepsilon_z/\varepsilon_\perp|}$ and $\omega d/c\ll v/c\ll1$, and there is actually no need to consider the additional condition of $v^2/c^2\ll|\varepsilon_z/\varepsilon_\perp|$. The underlying reason is that the factor $\left(1-\frac{v^2}{c^2}\varepsilon_\perp+\frac{\kappa_\perp^2v^2}{\omega^2}\frac{\varepsilon_\perp}{\varepsilon_z}\right)$ in all $a_{1|2}^{-,0}$, $a_{1|2}^{+,0}$ and $a_{2|3}^{-,0}$ in equations (S34-S36) can be cancelled out automatically

when considering the summation in equation (S33).

Section S6. Relative permittivity of hexagonal BN

In this work, hexagonal BN is chosen as the uniaxial material with a relative permittivity of $[\varepsilon_\perp, \varepsilon_\perp, \varepsilon_z]$. From previous works [54-60], the relative permittivity of BN can be expressed as

$$\varepsilon_\perp(\omega) = \varepsilon_\perp(\infty) + s_{\nu,\perp}\frac{\omega_{\nu,\perp}^2}{\omega_{\nu,\perp}^2 - i\gamma_{\nu,\perp}\omega - \omega^2} \tag{S42}$$

$$\varepsilon_z(\omega) = \varepsilon_z(\infty) + s_{\nu,z}\frac{\omega_{\nu,z}^2}{\omega_{\nu,z}^2 - i\gamma_{\nu,z}\omega - \omega^2} \tag{S43}$$

where $\varepsilon_\perp(\infty) = 4.87$, $\varepsilon_z(\infty) = 2.95$; $s_{\nu,\perp} = 1.83$ and $s_{\nu,z} = 0.61$ are the dimensionless coupling factors; $\hbar\omega_{\nu,\perp} = 170.1$ meV and $\hbar\omega_{\nu,z} = 92.5$ meV are the normal frequencies of vibration [54-60]; $\hbar\gamma_{\nu,\perp} = 0.87$ meV and $\hbar\gamma_{\nu,z} = 0.25$ meV are the amplitude decay rates.

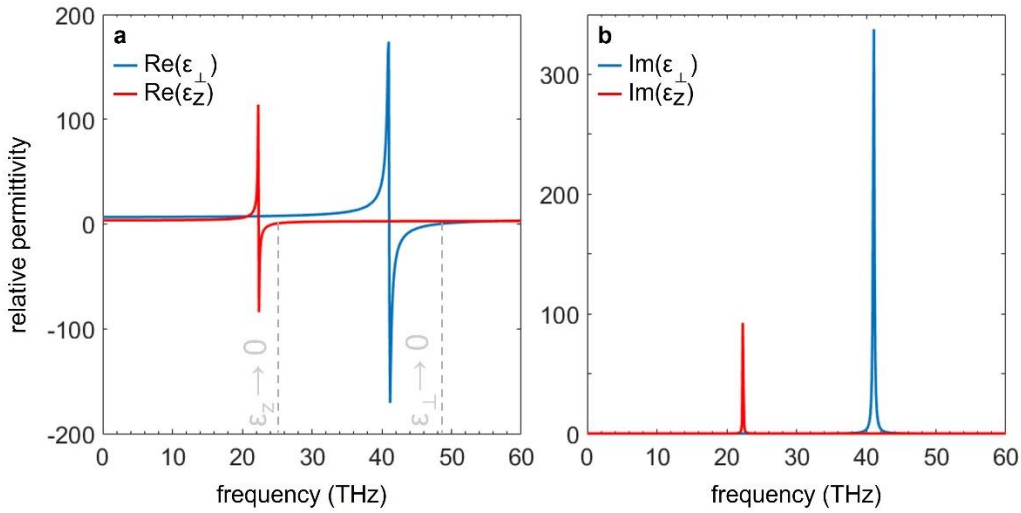

Figure S4. Relative permittivity of hexagonal BN. These curves are calculated according to equations (S42-S43).

The BN has two reststrahlen bands. To be specific, the first reststrahlen band of BN is within the range of 22.7-24.8 THz, in which the BN shows the optical response of type I hyperbolic materials; the second reststrahlen band of BN is within the range of 41.1-48.4 THz, in which the BN behaves like a type II hyperbolic material. Fig. S4 shows the relative permittivity of BN as a function of the frequency. At three representative frequencies studied in the main text, we have $\varepsilon_\perp = 7.7 + 0.01i$ and $\varepsilon_z = -0.05 + 0.04i$ at

24.5 THz (within the first reststrahlen band), $\varepsilon_\perp = -34.8 + 4.6i$ and $\varepsilon_z = 2.7 + 0.0005i$ at 42 THz (within the second reststrahlen band), and $\varepsilon_\perp = 11.6 + 0.1i$ and $\varepsilon_z = 2.5 + 0.001i$ at 35 THz (outside these two reststrahlen bands). In addition, we have $\varepsilon_\perp \to 0$ near 48.2 THz (namely $\varepsilon_\perp = 0.02 + 0.08i$ and $\varepsilon_z = 2.8 + 0.0003i$).

Section S7. Low-velocity-favored transition radiation from epsilon-near-zero materials with and without the existence of high-*k* modes

In this section, we show in Fig. S5 that the revealed phenomenon of low-velocity-favored transition radiation can also occur from an isotropic epsilon-near-zero material (e.g. $\varepsilon_\perp = \varepsilon_z = 0.05$ in Fig. S5a&d) and from a uniaxial epsilon-near-zero material with an elliptical isofrequency contour (e.g. $\varepsilon_\perp = 7.7$ and $\varepsilon_z = 0.05$ in Fig. S5b&e) without the existence of the mentioned high-*k* modes, in addition to that from a hyperbolic epsilon-near-zero material (e.g. $\varepsilon_\perp = 7.7$ and $\varepsilon_z = -0.05$ in Fig. S5c&f) with the existence of the mentioned high-*k* modes. This way, Fig. S5 indicates that the occurrence of low-velocity-favored transition radiation does not necessarily require the existence of high-*k* modes in epsilon-near-zero materials but is dependent on the value of $|\varepsilon_z|$. The underlying reason is that our revealed phenomenon in Fig. S5 is not caused by Cherenkov radiation of high-*k* modes (see more in Fig. S9) but related to the bulk-plasmon-mediated free-electron radiation beyond the conventional formation time as revealed in Ref. [4].

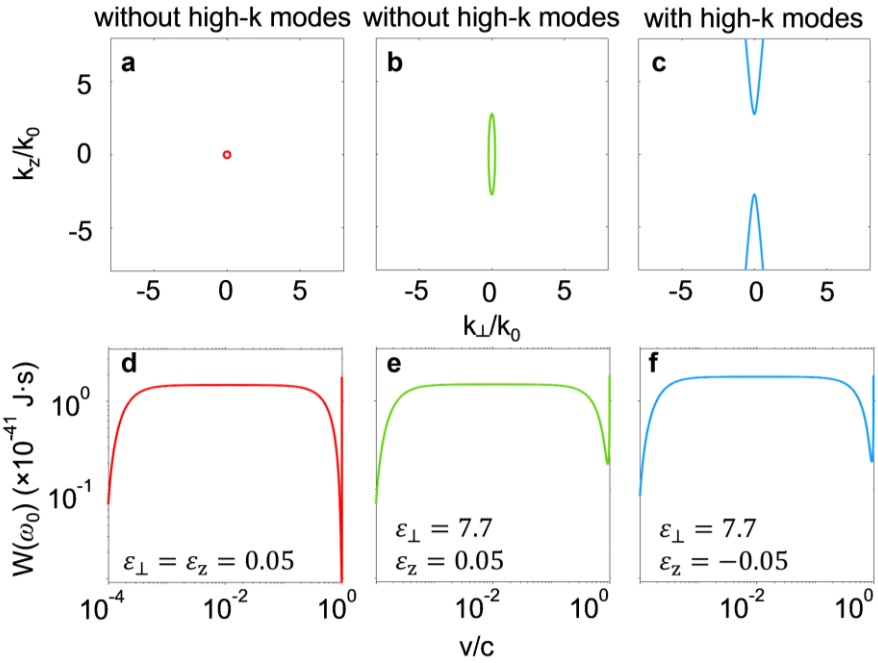

Figure S5. Low-velocity-favored transition radiation from various epsilon-near-zero materials with and without the existence of high-*k* modes. The structural setup is the same as Fig. 2 (e.g. the frequency

is 24.5 THz and the slab thickness is 1 nm), except for the relative permittivity $[\varepsilon_\perp, \varepsilon_\perp, \varepsilon_z]$ of epsilon-near-zero materials. (**a-c**) Isofrequency contour of eigenmodes inside the epsilon-near-zero material. For illustration, the material loss is neglected in this figure, and we set $\varepsilon_\perp = \varepsilon_z = 0.05$ in (a), $\varepsilon_\perp = 7.7$ & $\varepsilon_z = 0.05$ in (b), and $\varepsilon_\perp = 7.7$ & $\varepsilon_z = -0.05$ in (c). Accordingly, the high-k modes do not exist in (a,b) and appear only in (c). (**d-f**) Radiation spectrum of transition radiation from the corresponding three types of epsilon-near-zero materials in (a-c). The phenomenon of low-velocity-favored transition radiation appears in all three cases studied in (d-f), as long as $|\varepsilon_z| \to 0$. This way, the occurrence of low-velocity-favored transition radiation does not necessarily require the existence of high-k modes in epsilon-near-zero materials.

Section S8. More discussion on Fig. 3 at 35 THz

This section serves as the supplementary information for Fig. 3. Fig. S6a shows the angular spectral energy density at 35 THz. Fig. S6b-c show the field distributions of the excited waves at the frequency of 35 THz without $\varepsilon_z \to 0$. The radiation performance at 35 THz in Fig. S6 is similar to that at 42 THz without $\varepsilon_z \to 0$ as shown in Fig. 3d-f. For example, the strength of the excited field with $v/c = 0.001$ in Fig. S6b is much weaker than that with $v/c = 0.999$ in Fig. S6c.

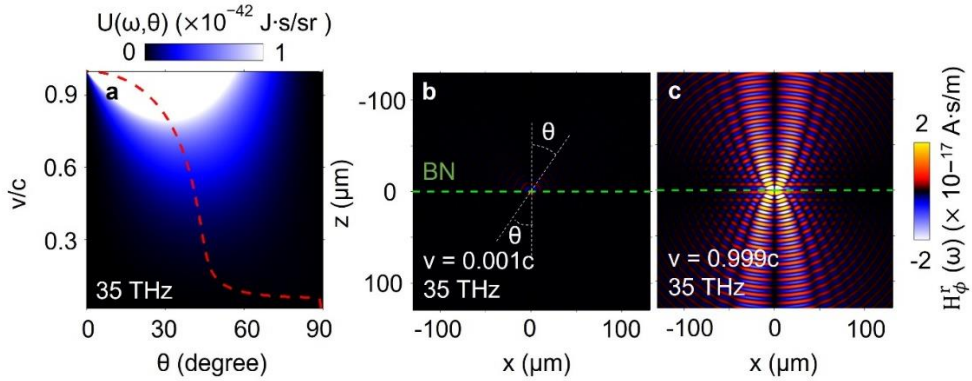

Figure S6. Angular spectral energy density and distribution of the excited magnetic field H_ϕ^r at different electron velocities at 35 THz. The other structural setup is the same as that in Fig. 3.

Section S9. Influence of the BN thickness on the low-velocity-favored transition radiation.

Due to these exotic features of transition radiation at 24.5 THz with $\varepsilon_z \to 0$, below we discuss the radiation performance at $\omega_0/2\pi$ =24.5 THz by investigating the influence of the slab thickness on the low-velocity-favored transition radiation in Fig. S7. Fig. S7a shows the total energy spectrum $W(\omega_0)$ as a function of the particle velocity by varying the slab thickness $d = d_j$ ($j = 1, 2$, or 3), namely from $d_1 = 1$ nm, $d_2 = 10$ nm to $d_3 = 100$ nm. For these three cases, the dependences of $W(\omega_0)$ on the electron velocity are similar in Fig. S7a. Particularly, $W(\omega_0)$ in Fig. S7a is insensitive to the variation of v, if $v \in [v_{A_1}, v_{B_1}]$ under the case of d_1, if $v \in [v_{A_2}, v_{B_2}]$ under the case of d_2, and if $v \in [v_{A_3}, v_{B_3}]$ under the case of d_2, where $v_{A_1}/c = 4.5 \times 10^{-4}$, $v_{A_2}/c = 4.5 \times 10^{-3}$, $v_{A_3}/c = 3.7 \times 10^{-2}$, $v_{B_1}/c = 0.26$, $v_{B_2}/c = 0.27$, and $v_{B_3}/c = 0.36$. This information is briefly summarized in Fig. S7b, where the value of v_{A_j} almost linearly increases with d_j. Moreover, Fig. S7a shows that the value of $W(\omega_0)$ with $v \in [v_{A_j}, v_{B_j}]$ is the same as that with $v = v_{D_j}$. By contrast, v_{D_j} is almost independent on d_j, as shown in Fig. S7b.

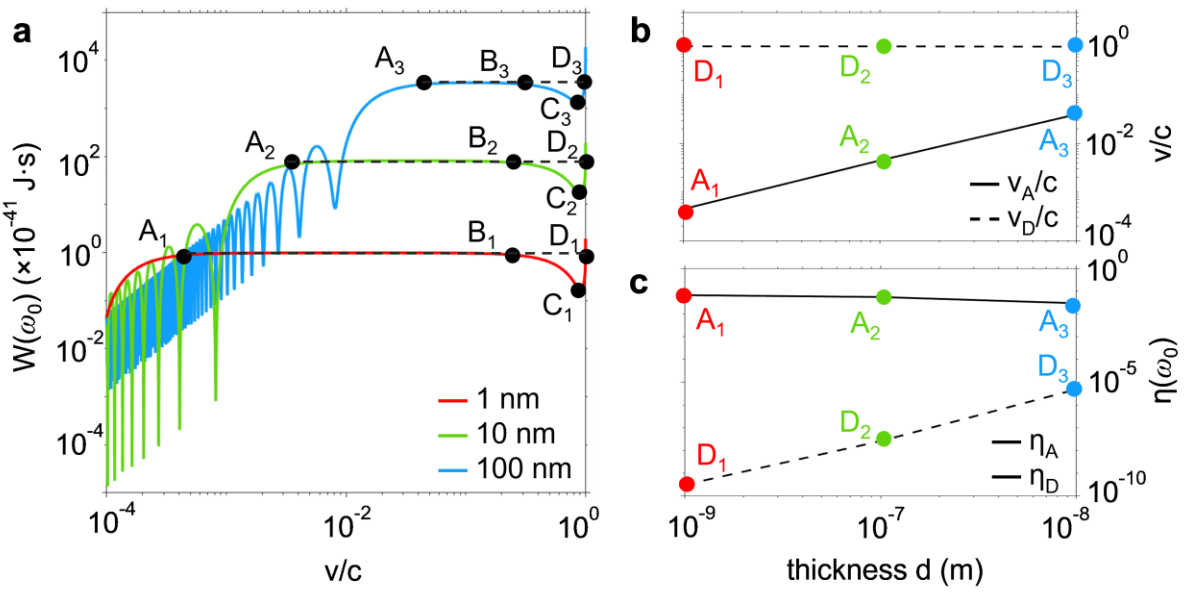

Figure S7. Influence of the BN thickness on the low-velocity-favored transition radiation. In this figure, the thickness $d = d_j$ ($j = 1, 2$ or 3) of the BN slab varies from $d_1 = 1$ nm, $d_2 = 10$ nm, to $d_3 = 100$ nm. The other structural setup is the same as that in Fig. 2. The working frequency is $\omega_0/2\pi = 24.5$ THz. (**a**) Radiation spectrum $W(\omega_0)$ of the excited propagating waves as a function of the electron velocity v at different thicknesses of the BN slab. The points of A_j and D_j have the same value of $W(\omega_0)$. (**b**) Extracted electron velocity v at the points of A_j and D_j in (a) as a function of d_j. (**c**) Extracted photon extraction

efficiency $\eta(\omega_0)$ at the points of A_j and D_j in (a) as a function of d_j. This figure serves as the supplementary information for Fig. 2b.

Fig. S7a also shows that $W(\omega_0)$ tends to increase with the slab thickness. To be specific, if $v \in [v_{A_j}, v_{B_j}]$, the value of $W(\omega_0)$ with $d_3 = 100$ nm is almost two (four) orders of magnitude higher than that with $d_2 = 10$ nm ($d_1 = 1$ nm). We then plot the photon extraction efficiency at points of A_j and D_j in Fig. S8c. From Fig. S7c, the value of $\eta(\omega_0)$ at points A_j is insensitive to the variation of d_j, due to the simultaneous increase of v_{A_j} and $W(\omega_0)$ with d_j in Fig. S7a&b. By contrast, the value of $\eta(\omega_0)$ at points D_j linearly increases with d_j, since v_{D_j} is insensitive to d_j but $W(\omega_0)$ at points D_j increases with d_j. In addition, Fig. S7a shows that the curve of $W(\omega_0)$ would oscillate with v, when $v/c < 10^{-3}$ under the case of d_2, or when $v/c < 10^{-2}$ under the case of d_3. This oscillation is due to the interference of transition radiation from the upper and lower boundaries of BN.

Section S10. Size of a hole through the BN slab

When a slow electron moves with a velocity $\overline{v} = \hat{z}v$ in free space, the wavevector of its carried evanescent waves at the frequency with $\varepsilon_z \to 0$ can be expressed as $\bar{k}_0 = \hat{\rho}k_\rho + \hat{z}k_z$, where $k_z = \omega_0/v$ due to the momentum match between the moving electron and the induced waves, $|\bar{k}_0| = k_0 = \omega_0/c$, and $\omega_0/2\pi = 24.5$ THz in this work. Mathematically, we have $k_\rho = \sqrt{k_0^2 - k_z^2} = ik_0\sqrt{1/\beta^2 - 1}$, where $\beta = v/c$; and we approximately have $k_\rho = ik_0/\beta$ for slow electrons with $\beta \ll 1$. Since k_ρ is a purely imaginary number, this indicates that the induced evanescent waves would decay with a factor of $e^{ik_\rho \rho}$ along the ρ direction. To enable sufficient interaction between the BN slab and the evanescent waves carried by slow electrons, the diameter d_{hole} of the hole through the BN slab should be small enough, for example, $\rho_{\text{hole}} \le 1/|k_\rho| = \beta/k_0 = \beta\lambda_0/(2\pi)$, where $\lambda_0 = 2\pi c/\omega_0 = 12$ μm. That is, it is better to let $d_{\text{hole}} \le 20$ nm if $\beta = 0.01$ and $d_{\text{hole}} \le 200$ nm if $\beta = 0.1$.

Section S11. Transition radiation from the BN slab near 48.2 THz

From Fig. S4, we also have $|\varepsilon_\perp| \to 0$ near 48.2 THz. To be specific, we have $\varepsilon_\perp = 0.02 + 0.08i$ and $\varepsilon_z = 2.8 + 0.0003i$ at 48.2 THz. We then plot in Fig. S8 the radiation spectrum as a function of the electron

velocity at 48.2 THz. Fig. S8 shows that when $v \in [v_A, v_B]$, the radiation intensity $W(\omega_0)$ at 24.5 THz with $|\varepsilon_z| \to 0$ is almost two orders of magnitude larger than that at 48.2 THz with $|\varepsilon_\perp| \to 0$, where $v_A/c = 0.4 \times 10^{-3}$ and $v_B/c = 0.29$. Besides, compared with 35 THz and 42 THz, the radiation intensity $W(\omega_0)$ at 48.2 THz does not show obvious enhancement. Therefore, we conclude that the phenomenon of low-velocity-favored transition radiation cannot occur near the frequency with $|\varepsilon_\perp| \to 0$ as shown in Fig. S8 but can only occur near the frequency with $|\varepsilon_z| \to 0$ as shown in Fig. 4b.

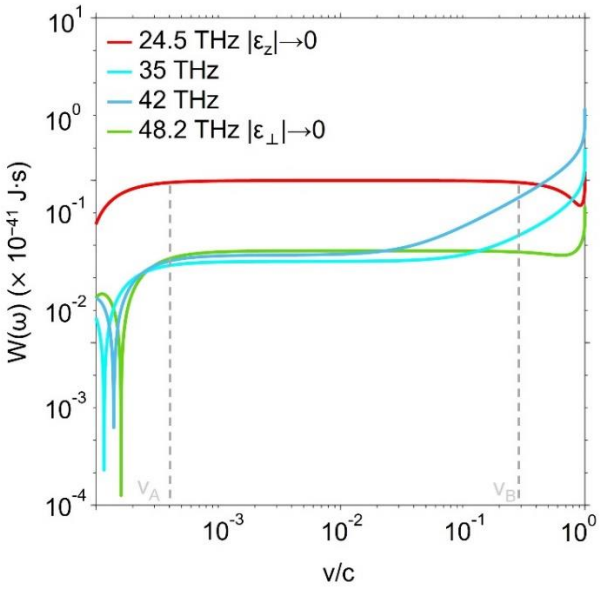

Figure S8. Low-velocity-favored transition radiation from the BN slab at 48.2 THz. The other structural setup is the same as that in Fig. 2b. This figure serves as the supporting information for Fig. 2b.

Section S12. Some discussion on the Cherenkov radiation

This work is analytically calculated within the framework of macroscopic Maxwell's equations and has already considered the Cherenkov radiation, including Fig. S7. We show in Fig. S9 that the contribution of Cherenkov radiation can be safely neglected in the whole excited propagating waves, due to the relatively-thin thickness of BN (e.g. 1-100 nm in Fig. S7) considered in this work.

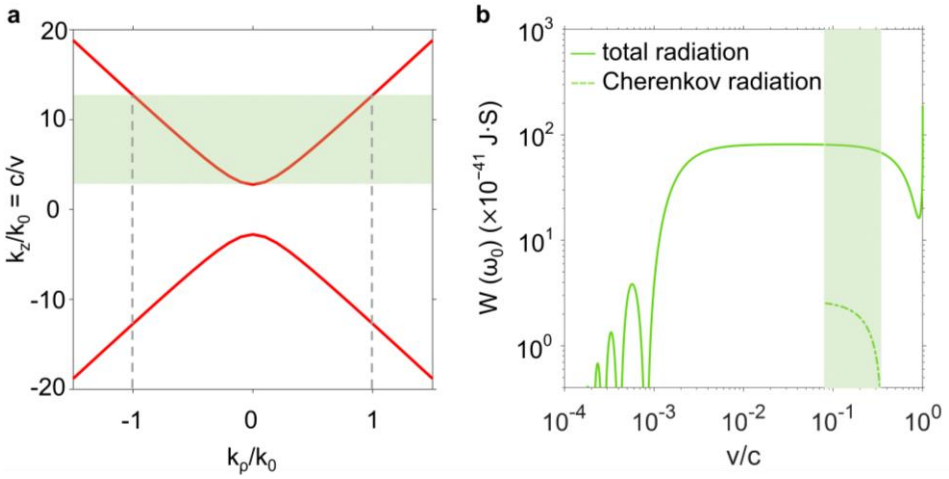

Figure S9. Some discussion on the Cherenkov radiation. (a) Dispersion of eigenmodes supported in a homogeneous infinitely-large BN at 24.5 THz, which has $\varepsilon_\perp = 7.7 + 0.01i$ and $\varepsilon_z = -0.05 + 0.04i$. Under this scenario, the iso-frequency contour is hyperbolic. Accordingly, if the electron moves along the z direction, the creation of Cherenkov radiation requires that $v \leq c/\sqrt{Re(\varepsilon_\perp)} = 0.36c$. On the other hand, the excited Cherenkov radiation should have $k_\rho/k_0 \leq 1$ so that it can be safely coupled out into free space without total internal reflection at the interface between BN and free space. This way, this condition further requires $v \geq 0.08c$. For clarity, the velocity regime with $0.08c \leq v \leq 0.36c$ has been highlighted with a green region. (b) Radiation spectrum of the Cherenkov radiation and the totally-excited propagating waves as a function of the electron velocity. For illustration, the thickness of BN is $d_{\mathrm{BN}} = 10$ nm in this figure. According to the Frank-Tamm formula for Cherenkov radiation, the radiation spectrum of Cherenkov radiation created inside the BN slab can be described by $W(\omega) = \frac{q^2 d_{\mathrm{BN}} \mu_0}{4\pi} \omega \left(1 - \frac{c^2}{v^2 n_{\mathrm{eff}}^2}\right)$ [29], where the effective index is $n_{\mathrm{eff}} = \sqrt{\varepsilon_z + (1 - \frac{\varepsilon_z}{\varepsilon_\perp})(\frac{c}{v})^2}$ [29]. Within the highlighted green region, the intensity of excited Cherenkov radiation is two orders of magnitude smaller than that of the totally-excited propagating waves, due to the relatively-thin thickness of BN considered in this work. This way, the contribution of Cherenkov radiation in this work can be safely neglected.

Section S13. Influence of the material loss on the low-velocity-favored transition radiation

The material loss would have a certain impact on the transition radiation. We show in Fig. S10 that under the existence of a reasonably-large material loss, the phenomenon of low-velocity-favored transition

radiation could exist. In addition, when the loss increases, the corresponding value of radiation spectrum $W(\omega)$ (e.g. within the velocity range of $v \in [v_A, v_B]$) would decrease in Fig. S10.

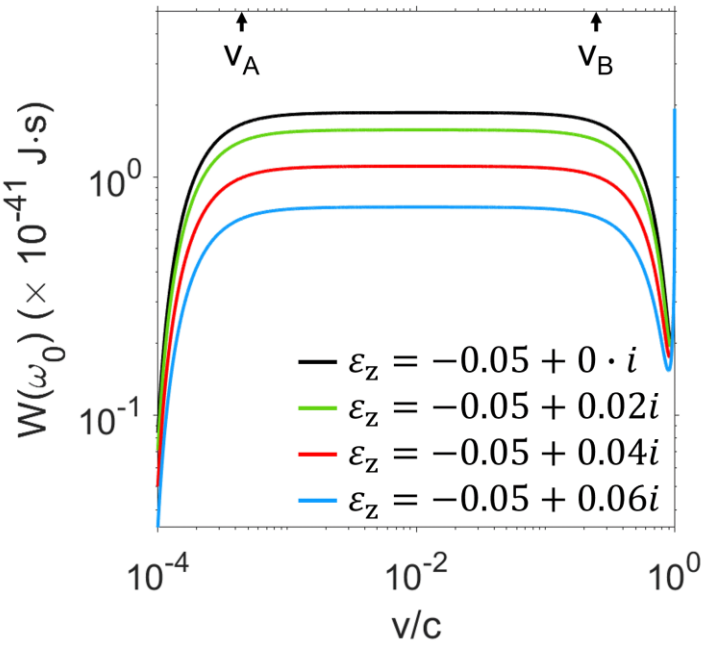

Figure S10. Influence of the material loss on the phenomenon of low-velocity-favored transition radiation. This figure serves as the complementary information for Fig. 4b. The structural setup is the same as Fig. 4b, except for the value of ε_z. As background, when considering the material loss of BN, we have $\varepsilon_z = -0.05 + 0.04i$ and $\varepsilon_\perp = 7.7 + 0.01i$ at the frequency of $\omega_0/2\pi = 24.5$ THz. When the value of $Im(\varepsilon_z)$ varies from 0, 0.02, 0.04, to 0.06, the phenomenon of low-velocity-favored transition radiation exists. The performance of this phenomenon would degrade when the loss increases. For example, the value of $W(\omega_0)$ within the range of $v \in [v_A, v_B]$ would decrease if the loss increases.